IFSCC 2025 full paper (IFSCC2025-211)

"Biohacking Molecular Aging: Unlocking the Power of RNA Nanoparticles to Combat Cellular Senescence and Restore Extracellular Homeostasis"

Sandra Freitas-Rodríguez [1], Christian Betancourt [2], Paula Vela Cristóbal [2], Ainhoa Díaz de Pedroviejo [2], Rebeca Alonso Bartolomé [2], Gabriel Bretones [3]

[1] R&D, Nanovex Biotechnologies SL, Llanera, [2] R&D, Nalón Innova SL, [3] Bioquímica y Biología Molecular, Universidad de Oviedo, Oviedo, Spain

1. Introduction

Aging is a complex biological process marked by the progressive accumulation of cellular and molecular damage that compromises tissue structure and function. It is driven by both intrinsic and extrinsic factors, including genetic alterations, oxidative stress, telomere shortening, and environmental exposure such as ultraviolet (UV) radiation, pollution, and lifestyle habits [9,17]. The skin, due to its constant exposure to external aggressors, is one of the most visibly affected organs. Hallmarks of skin aging include loss of elasticity, firmness, hydration, and the appearance of wrinkles and sagging [10,18].

At the cellular level, aging is largely mediated by senescence—a state of permanent cell cycle arrest triggered by stressors and regulated by pathways such as p53/p21 and p16INK4a/Rb [9,16]. Senescent cells remain metabolically active and acquire a pro-inflammatory profile known as the senescence-associated secretory phenotype (SASP), which alters the tissue microenvironment and impairs regeneration [4]. In the skin, the accumulation of senescent dermal fibroblasts contributes to extracellular matrix (ECM) degradation, affecting key structural proteins like collagen and elastin [8,15]. The ECM itself is a dynamic, highly organized 3D network that provides mechanical support and regulates cell behaviour; its dysregulation—primarily due to fibroblast senescence—is a hallmark of aging and a promising therapeutic target [8,9,18].

RNA-based therapies have emerged as powerful tools for gene modulation with high specificity. Messenger RNA (mRNA) therapies enable transient protein expression in target cells; however, the inherent instability of in vitro-transcribed mRNA in the presence of nucleases remains a challenge. This has led to the development of advanced delivery systems that enhance mRNA stability and translational efficiency [6,13]. Among these, lipid nanoparticles (LNPs)—clinically validated during the COVID-19 pandemic—offer protection, promote cellular uptake, and support effective gene expression in target tissues [1,7].

In this study, we hypothesized that overexpression of the transcription factor HES1, delivered via mRNA-loaded LNPs, could specifically target and reverse senescence in human dermal fibroblasts. Unlike conventional broad-spectrum cosmetic actives, our approach involves the

rational design of an mRNA-based agent that directly modulates key molecular pathways involved in cellular senescence. HES1 regulates cell fate and has been shown to modulate inflammation and senescence-associated signalling in skin models [16,18]. We designed, synthesized, and characterized LNPs encapsulating HES1 mRNA, and tested their effects using a replicative senescence model of human dermal fibroblasts. This model closely mimics physiological senescence associated with aging, providing a highly relevant platform for cosmetic innovation. Additionally, we propose performing transcriptomic screening to uncover how this novel active influences multiple senescence-related pathways, positioning it as a next-generation, mechanism-driven cosmetic strategy.

2. Materials and Methods

LNP Synthesis

LNPs were synthesized using the NanoScaler microfluidic system (Knauer) to ensure controlled particle size and encapsulation. The aqueous phase (mRNA in 100 mM acetate buffer) and organic phase (lipid mixture in ethanol, consisting of ionizable lipid, helper lipid, PEGylated lipid, and structural lipid) were combined via a cross-flow microfluidic setup at defined flow rate ratios (FRR) and total flow rates (TFR). Ethanol was removed by overnight dialysis at 4 °C in 1× PBS using 20 kDa cutoff cassettes. LNPs were stored at 4 °C.

Physicochemical Characterization

Particle size and polydispersity index (PDI) were determined by dynamic light scattering (DLS) using a NanoZS90 system (Malvern). Measurements were performed in triplicate for each formulation.

Encapsulation Efficiency

mRNA encapsulation efficiency (EE) was determined using the Quant-iT™ RiboGreen RNA assay kit (Invitrogen), following the manufacturer's protocol with minor modifications. Briefly, prior to the assay, samples were pre-diluted 1:25 in the assay matrix to minimize potential fluorescence interference and to ensure sample concentration fell within the linear range of the standard curve. A calibration curve was prepared using RNA standards diluted in TE 1× buffer, with and without 0.5% (v/v) Triton X-100 (Merck), to determine free and total RNA content, respectively.

Each sample was assayed in duplicate, with and without Triton X-100. In the absence of detergent, only free (non-encapsulated) RNA is detected, while the presence of Triton X-100 disrupts the LNPs, releasing encapsulated RNA and allowing quantification of total RNA content. Triton X-100 was prepared at 0.5% (v/v) from a 10% stock solution and added to the samples in a 1:1 ratio. All samples were incubated at 37 °C for 10 minutes prior to the addition of RiboGreen reagent, which was diluted 1:200 in TE buffer and added at 100 µL per well, bringing the final volume to 200 µL.

Fluorescence was measured using a Synergy HTX Multi-Mode Microplate Reader (BioTek) with excitation/emission wavelengths of 480/520 nm. RNA concentrations were interpolated from the standard curves to determine both free and total RNA. The encapsulated RNA was calculated as the difference between total and free RNA, and the encapsulation efficiency was calculated as:

$$\mathbf{EE\% = (Encapsulated\ RNA\ /\ Total\ RNA) \times 100}$$

Concentration and Purification

LNPs were concentrated using 50 kDa centrifugal filters (13,300 rpm, 4 °C) pre-equilibrated with PBS. Filtration was repeated in cycles until the desired volume was achieved.

Cell Culture and Senescence Induction

Human dermal fibroblasts (GM05565, Coriell Institute) were cultured in MEF medium (DMEM supplemented with 20% FBS, sodium pyruvate, HEPES, non-essential amino acids, and antibiotics) at 37 °C in 5% CO_2. Cells at passage 26 were used as a model of replicative senescence.

Transfection Protocol

Cells at 70–80% confluence were transfected with LNPs diluted in Opti-MEM for 12 h, followed by media replacement. Nuclear staining was performed using Hoechst (1 µg/mL), and fluorescence imaging was conducted with a Zeiss Axio Observer microscope at 10× magnification.

Senescence-Associated β-Galactosidase Assay

Senescence-associated β-galactosidase activity was measured using the Senescence β-Gal Staining Kit (Cell Signalling Technology) following the manufacturer's protocol. Cells were incubated overnight at 37 °C (CO_2-free), washed, and imaged.

RNA Extraction, RT-qPCR, and RNA-seq Analysis

Total RNA was extracted from monolayer cell cultures using TRIzol™ Reagent (Invitrogen), following the manufacturer's protocol. Briefly, cells were lysed in 1 mL of TRIzol and incubated for 5 minutes at room temperature. Subsequently, 200 µL of chloroform (Emsure) was added, mixed thoroughly, and the samples were centrifuged at 12,000 rpm for 15 minutes. The aqueous phase was transferred to a new RNase-free microcentrifuge tube and mixed with 500 µL of isopropanol (Emsure), followed by a 10-minute incubation and centrifugation at 12,000 rpm for 10 minutes. The RNA pellet was washed with 1 mL of 75% ethanol, centrifuged at 7,500 rpm for 5 minutes, and air-dried before resuspension in 20 µL of RNase-free water (Qiagen). RNA concentration and purity were assessed using a NanoDrop™ spectrophotometer (Thermo Fisher Scientific) by measuring absorbance at 260 nm.

For gene expression analysis, 1 µg of total RNA was reverse-transcribed into cDNA using the QuantiTect® Reverse Transcription Kit (Qiagen), following the manufacturer's instructions. Briefly, RNA was incubated with the gDNA Wipeout buffer at 42 °C for 2 minutes, followed by reverse transcription at 42 °C for 30 minutes and enzyme inactivation at 95 °C for 3 minutes. Quantitative real-time PCR (RT-qPCR) was performed using Power SYBR™ Green PCR Master Mix (Thermo Fisher Scientific) in 96-well plates using the 7300 Real-Time PCR System (Applied Biosystems). Reactions were run in duplicate in a final volume of 10 µL per well (2 µL cDNA, 0.5 µL each primer at 10 µM, 12.5 µL 2× SYBR mix, and nuclease-free water). The cycling program included initial denaturation (10 min at 95 °C), followed by 40 cycles of 15 s at 95 °C and 30 s at 57 °C, and a final melt curve analysis. Gene expression was normalized to ACTB using the ΔCt method:

$$\Delta Ct = 2^{(Ct_{ACTB} - Ct_{gene})}$$

For transcriptomic analysis, RNA-seq libraries will be prepared using the TruSeq Stranded mRNA Library Prep Kit (Illumina) and sequenced on a NovaSeq X platform (Illumina) with 150-bp paired-end reads (2×150 bp), aiming to generate approximately 60 million reads per

sample (~9 Gb/sample). Subsequent bioinformatic analyses will include read alignment, quantification of gene expression, and differential expression analysis (DEG).

Statistical Analysis

All experiments were conducted in biological triplicates. Statistical analysis was performed using two-way ANOVA (GraphPad Prism v10.0), with $p < 0.05$ considered statistically significant.

3. Results

3.1. LNPs Encapsulating Reporter mRNAs Demonstrate Efficient Cellular Deliver

As outlined in the introduction, this study aimed to reverse cellular senescence in dermal fibroblasts through the overexpression of HES1 using mRNA-loaded lipid nanoparticles (LNPs). Prior to evaluating the functional delivery of HES1, the transfection efficiency and overall performance of the LNP delivery platform were validated using two fluorescent reporter mRNAs: mCherry and eGFP.

LNPs encapsulating these reporter mRNAs were successfully synthesized and characterized in terms of particle size, PDI, EE%, and mRNA content **(Table 1).** The formulation process yielded uniform nanoparticles with high EE% for both reporters.

Table 1. Size, PDI and EE% values of LNPs 24 h post-dialysis

Formulation	Size (nm)	PDI	EE (%)	µg/mL of mRNA encapsulated
LNPs ø	66.84 ± 1.11	0.257 ± 0.01	-	-
LNPs mCherry mRNA	64.61 ± 0.45	0.251 ± 0.01	96.7	33.2
LNPs eGFP mRNA	70.73 ± 1.21	0.243 ± 0.01	96.5	24.0

Ø: Empty LNPs; PDI: Polydispersity Index; EE: Encapsulation Efficiency; SD: Standard Deviation. Data are expressed as mean ± SD (n = 3).

Following synthesis, reporter-loaded LNPs were transfected into human dermal fibroblasts. Fluorescence imaging was performed 24 hours post-transfection to assess cellular uptake and protein expression **(Figure 1)**. The mCherry reporter was used to confirm the general functionality of the delivery system, acting as a proof-of-concept for mRNA-mediated expression *in vitro*. In parallel, eGFP mRNA was employed due to its future use as a fluorescent fusion tag for HES1 in downstream experiments, enabling visualization of intracellular localization and expression patterns. This dual-reporter validation step was essential to ensure the reliability of the LNP platform before proceeding with mechanistic studies involving HES1.

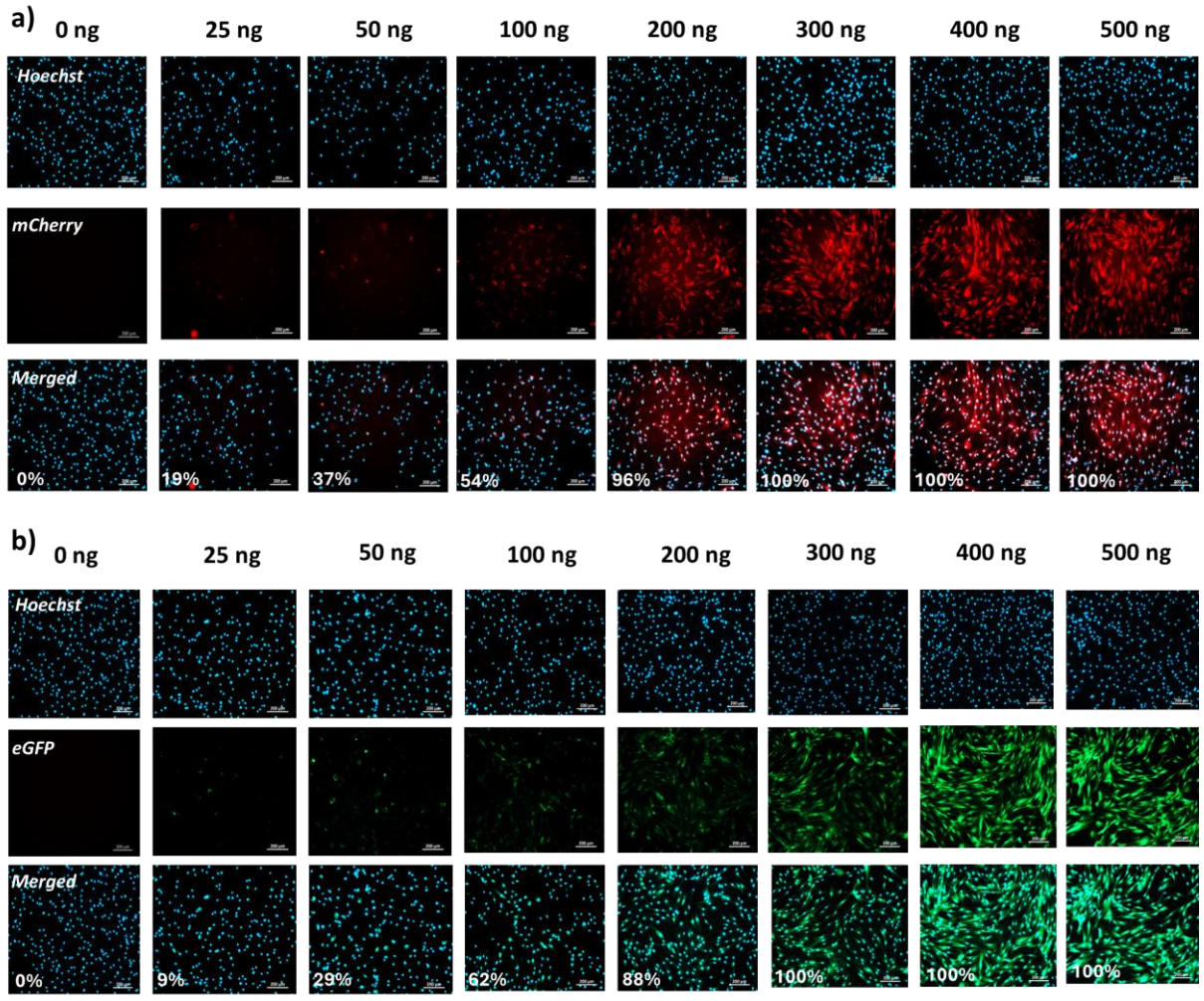

Figure 1. In vitro transfection of human dermal fibroblasts (p15) with (a) LNPs-mCherry mRNA and (b) LNPs-eGFP mRNA. Nuclei were stained with Hoechst. Scale bar = 200 µm.

Both reporter-loaded formulations demonstrated efficient intracellular delivery and robust expression of the corresponding fluorescent proteins in human dermal fibroblasts, with near-complete transfection observed at doses equal to or above 200 ng of mRNA per well **(Figure 1)**. Fluorescence was homogeneously distributed across the cell population, indicating consistent uptake and translation efficiency. These results confirmed the suitability of the LNP platform for mRNA delivery in vitro and provided a solid foundation for subsequent functional assays involving HES1.

3.2. LNPs Enable HES1 mRNA Overexpression in Senescent Dermal Fibroblasts

After validating the system, LNPs encapsulating HES1-eGFP mRNA were synthesized and characterized **(Table 2)**.

Table 2. Size, PDI and EE% values of LNPs 24 h post-dialysis

Formulation	Size (nm)	PDI	EE (%)	µg/mL of mRNA encapsulated
LNPs ø	69.24 ± 1.14	0.241 ± 0.01	-	-
LNPs HES1-eGFP mRNA	75.75 ± 0.88	0.221 ± 0.02	96.3	138.3

Ø: Empty LNPs; PDI: Polydispersity Index; EE: Encapsulation Efficiency; SD: Standard Deviation. Data are expressed as mean ± SD (n = 3).

Initial transfections with HES1-eGFP mRNA at reporter-level doses did not yield detectable fluorescence, suggesting that the amount of mRNA delivered was insufficient to achieve functional protein expression. Since HES1 is a nuclear transcription factor and may require higher expression levels to elicit detectable activity or localization, we hypothesized that an increased mRNA dose would enhance signal detection. To test this, a new batch of HES1-eGFP LNPs was synthesized and concentrated using ultrafiltration systems, thereby increasing the effective mRNA concentration for transfection. Fluorescence imaging performed 24 hours post-transfection confirmed successful expression of the HES1-eGFP fusion protein at these elevated doses, as shown in **Figure 2.**

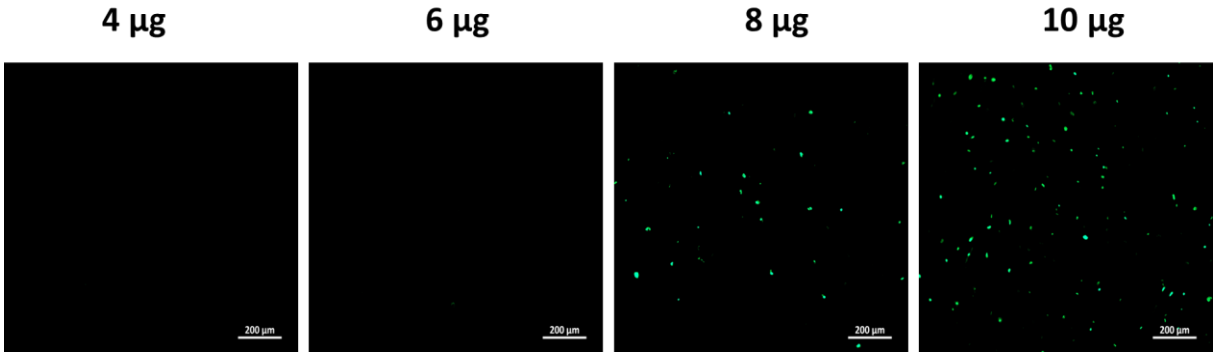

Figure 2. HES1-eGFP expression in senescent dermal fibroblasts (p26) after transfection with concentrated LNPs. Scale bar = 200 µm.

This confirmed that delivery of 8–10 µg of encapsulated HES1 mRNA significantly improved HES1 overexpression in our cellular model.

3.3. HES1 Overexpression Modulates Classical Senescence-associated Markers

Once HES1 overexpression was confirmed, cells were maintained under treatment for one week. After this period, cells were fixed with formaldehyde, a β-galactosidase assay was performed, and images were acquired as shown in **Figure 3.**

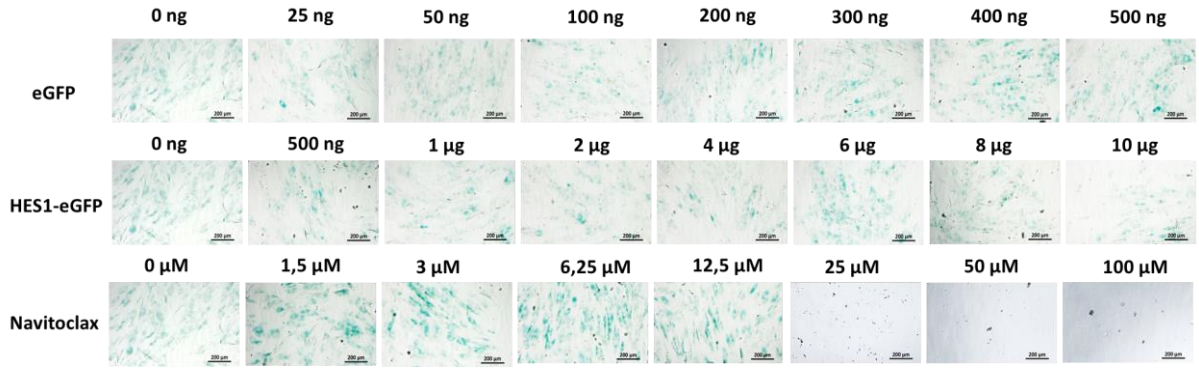

Figure 3. β-Galactosidase staining in fibroblasts treated with test compounds. HES1-treated cells show reduced staining. Scale bar = 200 µm.

A decrease in senescence-associated β-galactosidase (SA-β-gal) activity was observed in fibroblasts treated with 10 µg of HES1 mRNA, suggesting a potential senescence-reversing effect. As expected, the senolytic agent Navitoclax induced marked cell death at

concentrations ≥25 µM, in line with its reported activity. In parallel, the impact of HES1 mRNA on cellular senescence was compared with that of other cosmetic actives previously reported to exhibit senolytic activity in skin. Although these compounds showed partial efficacy in reducing SA-β-gal activity, they were associated with notable cytotoxicity at concentrations required for senescence modulation (data not shown). In contrast, HES1 mRNA significantly decreased SA-β-gal activity without compromising cell viability, supporting its potential as a safer and more targeted alternative for cosmetic applications focused on senescence.

To further investigate the molecular effects of HES1 overexpression, RT-qPCR was performed one-week post-treatment to assess the expression of senescence-related genes. The experimental groups included: (i) untreated control cells, (ii) cells transfected with LNPs encapsulating eGFP mRNA (300 ng/well, a dose at which nearly all fibroblasts were successfully transfected), and (iii) cells transfected with LNPs containing HES1-eGFP mRNA (10 µg/well, a dose shown to result in detectable HES1 expression via fluorescence imaging). This design enabled a direct comparison between baseline senescence levels, the potential impact of transfection alone, and the specific effect of HES1 overexpression.

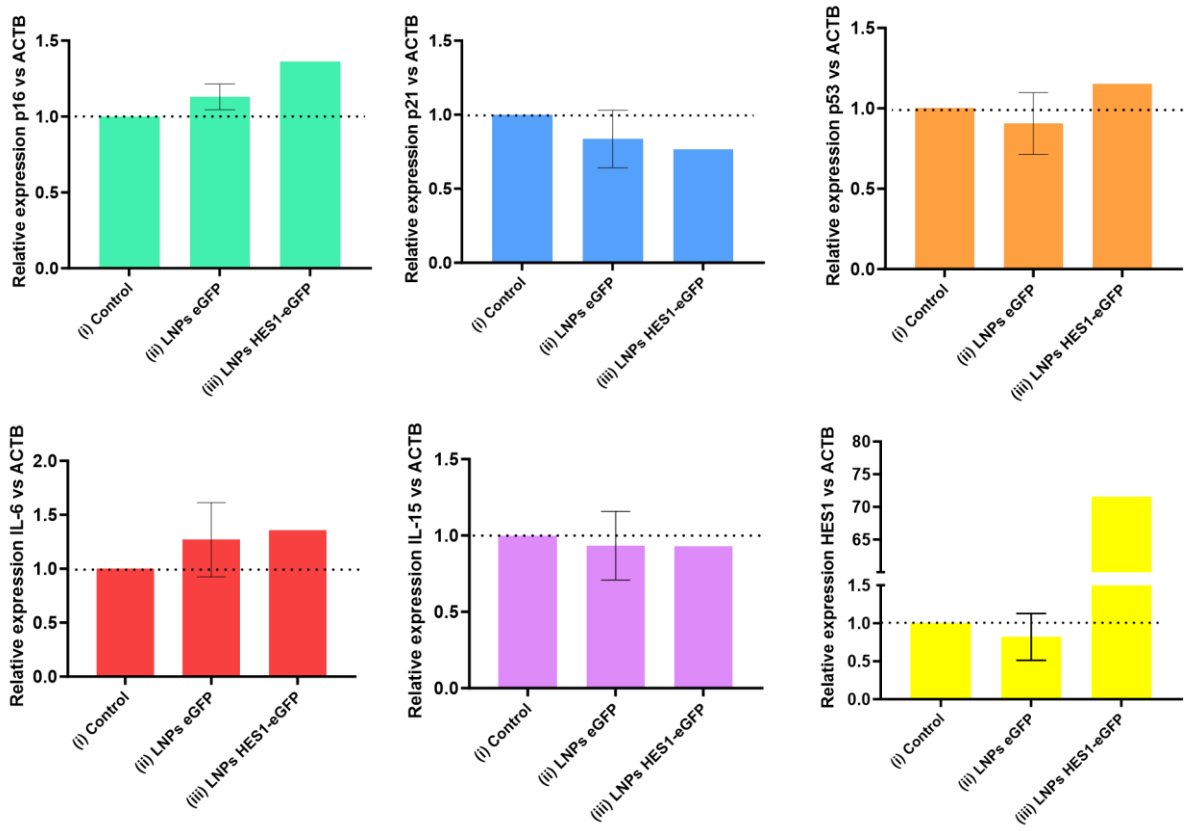

Figure 4. RT-qPCR analysis of senescence-related genes. Relative gene expression was calculated using the $2^{-\Delta\Delta Ct}$ method. HES1 expression is significantly upregulated, while p21 is downregulated, with modest changes observed in p16 and IL-6. Bars represent mean values; error bars indicate standard deviation (SD) when applicable.

As shown in **Figure 4,** RT-qPCR analysis revealed robust overexpression of HES1—approximately 70-fold—compared to both untreated cells and those transfected with eGFP mRNA. This upregulation was accompanied by a slight downregulation of p21, a key regulator of cell cycle arrest and senescence. In contrast, p16 and IL-6 were modestly upregulated, while p53 and IL-15 expression levels remained stable. These results reflect a complex transcriptional response to HES1 overexpression, suggestive of partial modulation of the senescent phenotype.

3.4. Transcriptomic Strategy for Mechanistic Insights

To explore the molecular consequences of HES1 overexpression in senescent dermal fibroblasts, a transcriptomic analysis was undertaken. This approach seeks to identify the signalling pathways and gene networks that are differentially regulated in response to HES1 expression. RNA-seq experiments have already been performed and are currently undergoing. The goal is to map transcriptional changes and gain insights into the molecular processes potentially influenced by HES1. These findings will later be validated through complementary *in vitro* assays and reconstructed skin models.

4. Discussion

The synthesis and characterization of the LNPs confirmed the suitability of microfluidic systems for generating nanoparticles with favourable physicochemical properties. The LNPs exhibited diameters below 200 nm, low polydispersity (PDI < 0.3), and high encapsulation efficiencies (EE% > 80%), as summarized in **Tables 1 and 2**, indicating robust stability and functionality. These results are consistent with previous reports demonstrating the effectiveness of lipid-based carriers for nucleic acid delivery [5,14].

To assess the functionality of the delivery system, transfection efficiency was evaluated in human dermal fibroblasts (GM05565). This model is particularly relevant as it closely mimics physiological senescence associated with aging, thereby providing a robust platform for cosmetic innovation. As shown in **Figure 1**, the LNPs achieved near-complete transfection at mRNA doses of 200 ng/well. Further supporting this, **Figure 2** illustrates that lower mRNA doses led to minimal fluorescence, confirming that higher concentrations are needed to attain functional protein expression [12].

To evaluate the biological relevance of this transfection strategy, we next examined its potential to modulate senescence pathways and compared it with a known senolytic agent. The senolytic effect of Navitoclax, shown in **Figure 3**, was evident at concentrations ≥25 µM, in agreement with its established capacity to eliminate senescent cells [2]. In parallel, treatment with 10 µg of HES1-eGFP mRNA induced strong HES1 overexpression, as confirmed by eGFP signal intensity. RT-qPCR data **(Figure 4)** showed that this overexpression correlated with a marked reduction in SA-β-gal staining and a modest downregulation of p21. Interestingly, p16 and IL-6 were modestly upregulated, while p53 and IL-15 remained largely unchanged. These findings are in partial alignment with previous studies supporting an anti-senescent role for HES1 [3,11]. Zou et al. (2021) [17] notably reported reduced HES1 levels in fibroblasts from aged donors, suggesting that restoring HES1 expression may counteract aspects of cellular aging.

In this context, our approach—based on LNP-mediated delivery of HES1 mRNA—demonstrated not only efficacy but also selectivity in modulating senescence-associated molecular pathways. Compared to other commonly used cosmetic actives, which in prior *in vitro* studies showed cytotoxic effects even at manufacturer-recommended doses, this strategy stands out for its ability to modulate cellular function without compromising cell viability. This contrast underscores the potential limitations of conventional extract-based actives, which often lack molecular specificity and reproducibility.

The observed trends in senescence markers require further validation with additional replicates and expanded statistical analyses. Current follow-up experiments include transcriptomic profiling via RNA-seq and qPCR validation to confirm HES1-driven gene expression changes. Importantly, the reproducibility of HES1 overexpression at 10 µg has been confirmed in repeated assays.

Future studies should explore the impact of HES1 overexpression on extracellular matrix components such as collagen and elastin, as well as evaluate its therapeutic potential in *ex vivo* human skin models. These approaches will further clarify both the efficacy of the mRNA payload and the targeting capability of the LNP delivery system.

Beyond highlighting the potential of HES1 as a novel, specific active against cellular senescence, our findings underscore the broader value of the LNP-based delivery platform. This technology not only enables efficient encapsulation and protection of labile biomolecules but also facilitates the rapid and rational design of tailored therapeutic strategies—allowing for targeted modulation of physiological processes through protein replacement approaches. Altogether, this work lays the foundation for innovative interventions in regenerative medicine and dermatological therapy, marking a shift toward next-generation actives with molecular precision.

5. Conclusions

1. LNPs synthesised using microfluidic methods, demonstrated physicochemical properties suitable for topical application and effectively encapsulated and delivered mRNA under in vitro conditions.
2. Encapsulation of HES1 mRNA in LNPs enabled successful overexpression of the transcription factor in human senescent dermal fibroblasts (GM05565 line).
3. HES1 overexpression achieved via LNP delivery resulted in a consistent and robust modulation of key senescence markers in human dermal fibroblasts, outperforming conventional actives in both efficacy and cellular tolerability. These findings support its potential as a highly specific and well-tolerated strategy for targeting cellular aging in cosmetic applications.
4. Beyond the specific case of HES1, the LNP-based mRNA delivery platform demonstrates strong potential as a versatile tool for the rational design of cosmetic actives aimed at modulating physiological processes with high specificity and adaptability.

6. References

1. Bost, J. P., Barriga, H., Holme, M. N., Gallud, A., Maugeri, M., Gupta, D., Lehto, T., Valadi, H., Esbjörner, E. K., Stevens, M. M., & El-Andaloussi, S. (2021). Delivery of Oligonucleotide Therapeutics: Chemical Modifications, Lipid Nanoparticles, and Extracellular Vesicles. ACS Nano, 15(9), 13993-14021. https://doi.org/10.1021/acsnano.1c05099
2. Chang, J., Wang, Y., Shao, L., Laberge, R.-M., Demaria, M., Campisi, J., Janakiraman, K., Sharpless, N. E., Ding, S., Feng, W., Luo, Y., Wang, X., Aykin-Burns, N., Krager, K., Ponnappan, U., Hauer Jensen, M., Meng, A., & Zhou, D. (2016). Clearance of senescent cells by ABT263 rejuvenates aged hematopoietic stem cells in mice. Nature Medicine, 22(1), 78–83. https://doi.org/10.1038/nm.4010
3. Coller, H. A., Sang, L., & Roberts, J. M. (2006). A New Description of Cellular Quiescence. *PLOS Biology, 4*(3), e83. https://doi.org/10.1371/journal.pbio.0040083
4. Freitas-Rodríguez, S., Folgueras, A. R., & López-Otín, C. (2017). The role of matrix metalloproteinases in aging: Tissue remodeling and beyond. *Biochimica Et Biophysica Acta. Molecular Cell Research, 1864*(11 Pt A), 2015–2025. https://doi.org/10.1016/j.bbamcr.2017.05.007

5. Godbout, K., & Tremblay, J. P. (2022). Delivery of RNAs to Specific Organs by Lipid Nanoparticles for Gene Therapy. Pharmaceutics, 14(10), Article 10. https://doi.org/10.3390/pharmaceutics14102129
6. Goss, D. J., & Domashevskiy, A. V. (2016). Messenger RNA (mRNA): The Link between DNA and Protein. In R. A. Bradshaw & P. D. Stahl (Eds.), *Encyclopedia of Cell Biology* (pp. 341–345). Academic Press. https://doi.org/10.1016/B978-0-12-394447-4.10040-9
7. Hou, X., Zaks, T., Langer, R., & Dong, Y. (2021). Lipid nanoparticles for mRNA delivery. Nature Reviews Materials, 6(12), Article 12. https://doi.org/10.1038/s41578-021-00358-0.
8. Huang, J., Heng, S., Zhang, W., Liu, Y., Xia, T., Ji, C., & Zhang, L. (2022). Dermal extracellular matrix molecules in skin development, homeostasis, wound regeneration and diseases. *Seminars in Cell & Developmental Biology, 128*, 137–144. https://doi.org/10.1016/j.semcdb.2022.02.027
9. López-Otín, C., Blasco, M. A., Partridge, L., Serrano, M., & Kroemer, G. (2023). Hallmarks of aging: An expanding universe. *Cell, 186*(2), 243–278. https://doi.org/10.1016/j.cell.2022.11.001
10. Lynch, B., Pageon, H., Le Blay, H., Brizion, S., Bastien, P., Bornschlögl, T., & Domanov, Y. (2022). A mechanistic view on the aging human skin through ex vivo layer-by-layer analysis of mechanics and microstructure of facial and mammary dermis. *Scientific Reports, 12*(1), 849. https://doi.org/10.1038/s41598-022-04767-1
11. Marthandan, S., Priebe, S., Hemmerich, P., Klement, K., & Diekmann, S. (2014). Long-Term Quiescent Fibroblast Cells Transit into Senescence. *PLoS ONE, 9*(12), e115597. https://doi.org/10.1371/journal.pone.0115597
12. Massaro, M., Wu, S., Baudo, G., Liu, H., Collum, S., Lee, H., Stigliano, C., Segura-Ibarra, V., Karmouty-Quintana, H., & Blanco, E. (2023). Lipid nanoparticle-mediated mRNA delivery in lung fibrosis. *European Journal of Pharmaceutical Sciences, 183*, 106370. https://doi.org/10.1016/j.ejps.2023.106370
13. Qin, S., Tang, X., Chen, Y., Chen, K., Fan, N., Xiao, W., Zheng, Q., Li, G., Teng, Y., Wu, M., & Song, X. (2022). mRNA-based therapeutics: Powerful and versatile tools to combat diseases. *Signal Transduction and Targeted Therapy, 7*(1), 1–35. https://doi.org/10.1038/s41392-022-01007-w
14. Sanghani, A., Kafetzis, K. N., Sato, Y., Elboraie, S., Fajardo-Sanchez, J., Harashima, H., Tagalakis, A. D., & Yu-Wai-Man, C. (2021). Novel PEGylated Lipid Nanoparticles Have a High Encapsulation Efficiency and Effectively Deliver MRTF-B siRNA in Conjunctival Fibroblasts. *Pharmaceutics, 13*(3), 382. https://doi.org/10.3390/pharmaceutics13030382
15. Statzer, C., Park, J. Y. C., & Ewald, C. Y. (2023). Extracellular Matrix Dynamics as an Emerging yet Understudied Hallmark of Aging and Longevity. *Aging and Disease, 14*(3), 670–693. https://doi.org/10.14336/AD.2022.1116
16. Wyles, S. P., Carruthers, J. D., Dashti, P., Yu, G., Yap, J. Q., Gingery, A., Tchkonia, T., & Kirkland, J. (2023). Cellular Senescence in Human Skin Aging: Leveraging Senotherapeutics. *Gerontology, 70*(1), 7–14. https://doi.org/10.1159/000534756
17. Zhang, J., Yu, H., Man, M.-Q., & Hu, L. (2023). Aging in the dermis: Fibroblast senescence and its significance. *Aging Cell*, e14054. https://doi.org/10.1111/acel.14054
18. Zou, Z., Long, X., Zhao, Q., Zheng, Y., Song, M., Ma, S., Jing, Y., Wang, S., He, Y., Esteban, C. R., Yu, N., Huang, J., Chan, P., Chen, T., Izpisua Belmonte, J. C., Zhang, W., Qu, J., & Liu, G.-H. (2021). A Single-Cell Transcriptomic Atlas of Human Skin Aging. *Developmental Cell, 56*(3), 383–397.e8. https://doi.org/10.1016/j.devcel.2020.11.002